

Whole-brain modeling of the differential influences of Amyloid-Beta and Tau in Alzheimer's Disease

Gustavo Patow^{1,4}, Leon Stefanovski^{2,3}, Petra Ritter^{2,3}, Gustavo Deco⁴ and Xenia Kobeleva^{5,6},
for the Alzheimer's Disease Neuroimaging Initiative*

Abstract

Alzheimer's Disease (AD) is a neurodegenerative condition associated with extra- and intra-neuronal accumulation of two misfolded proteins, namely Amyloid-Beta ($A\beta$) and tau. In this paper, we study the effect of these proteins on neuronal activity, with the aim of assessing their individual and combined impact on neuronal processes. The technique uses a whole-brain dynamic model to find the optimal parameters that best describe the effects of $A\beta$ and tau on the excitation-inhibition balance of the local nodes. Our experimental results show a clear dominance of the neuronal activity of $A\beta$ over tau in the early disease stages (Mild Cognitive Impairment), while tau dominates over $A\beta$ in the latest stages (AD). Our findings identify a crucial role for $A\beta$ and tau in contributing to complex neuronal dynamics and demonstrate the viability of using regional distributions of neuropathology to define models of large-scale brain function in AD. Our study provides further insight into the dynamics and complex interplay between these two proteins among themselves and with the regional neural activity, opening the path for further investigations on biomarkers and candidate therapeutic targets in-silico.

Keywords

Alzheimer's Disease — Whole-Brain model — Amyloid-Beta — Tau

¹ ViRVIG, Universitat de Girona, Girona, Spain

² Berlin Institute of Health at Charité – Universitätsmedizin Berlin, Berlin, Germany

³ Department of Neurology with Experimental Neurology, Brain Simulation Section, Charité – Universitätsmedizin Berlin, corporate member of Freie Universität Berlin and Humboldt-Universität zu Berlin, Berlin, Germany

⁴ Center for Brain and Cognition, Computational Neuroscience Group, Department of Information and Communication Technologies, Universitat Pompeu Fabra, Spain

⁵ University Hospital Bonn, Clinic for Neurology, Bonn, Germany

⁶ German Center for Neurodegenerative Diseases (DZNE) Bonn, Bonn, Germany

Corresponding author: Gustavo Patow, ViRVIG, Universitat de Girona, 17003, Spain. gustavo.patow@udg.edu

1. Introduction

Alzheimer's Disease (AD) is a neurodegenerative disease that affects first the medial temporal lobe and the limbic system, and most areas of the neocortex at later disease stages [1, 2, 3]. The disease can remain asymptomatic for years but ultimately leads to progressive impairment of memory and other cognitive domains, neuropsychiatric symptoms and, ultimately, to severe impairment in all body functions. This results in both a huge loss of quality of life of affected people and caregivers and high costs for the society at large. Minor cognitive deficits with little influence on activities of daily living with, are defined as mild cognitive impairment (MCI). In the typical disease course, the deficits extend later on to other cognitive domains as, e.g., speech and spatial orientation. When the cognitive impairment is severe enough to affect the activities of daily living, the disease is usually referred to as dementia (due to AD) [4].

AD pathogenesis is associated with several interlinked pathomechanistic processes, from genomics to connectomics, including the Notch-1 pathway, neurotransmitters, polygenetic factors, neuroinflammation, and neuroplasticity [5]. However, the accumulation of misfolded proteins within the brain is considered as the pathological hallmark of AD: namely extracellular accumulation of Amyloid-beta ($A\beta$), forming what are known as senile plaques; and intraneuronal aggregation of the microtubule protein tau, called neurofibrillary tangles [6]. In general, it is known that $A\beta$ plaques and tau tangles spread independently through the brain as the disease progresses [7]. Both proteins are currently considered as biomarkers that are used in the diagnostic classification of AD [6]. Although a plethora of treatment strategies has been examined in the last decades, the neuronal degeneration itself, as well as the cognitive decline cannot be currently stopped by any treatment, AD is therefore still considered as incurable. Treatments for removal of $A\beta$ (e.g., with Adacanumab and Lecanemab) are currently discussed in light of inconclusive effects on halting disease progression [8]. Even more, in spite of the large body of research devoted to the study of AD, many aspects regarding AD pathophysiology and the role of $A\beta$ and tau in the disease process are still incompletely understood [9, 10, 11]. While several studies have shown abnormal brain network function at various stages of AD [6, 12, 13], the relationship between pathology (i.e., $A\beta$ and tau) and associated brain dysfunction has not been described in great detail [10].

Regarding brain dysfunction, several ex-vivo (human) and animal studies have seen a disruption in excitation/inhibition (E/I) balance (i.e., the relative contributions of excitatory and inhibitory synaptic inputs corresponding to a neuronal event, such as a response evoked by sensory stimulation) in the form of hyperexcitability consequence of the disruption of glutamate reuptake, also disrupting cognition-related cortical activity and contributing to intellectual decline in AD [12, 13]. Change et al. [14] showed tau affects excitatory and inhibitory neurons differently, and that its ablation decreases the baseline activity of excitatory neurons, while modulating the intrinsic excitability and axon initial segments of inhibitory neurons, promoting network inhibition. In this line, Bi and co-workers [15] hypothesized that $A\beta$ produces alterations to the GABAergic system contributing to impairing GABAergic function and thus producing synaptic hyperexcitation, leading to E/I imbalance and AD pathogenesis. Petrache et al. [16] found a decrease in canonical synaptic signaling mechanisms first affecting the lateral entorhinal cortex in combination with synaptic hyperexcitation and severely disrupted E/I inputs onto principal cells, and a reduction in the somatic inhibitory axon terminals in the lateral entorhinal cortex compared with other cortical regions. Recently, Lauterborn and coauthors [17] studied the synaptic disturbances in E/I balance in forebrain circuits by assessing anatomical and electrophysiological synaptic E/I ratios in post-mortem parietal cortex samples of AD patients, revealing significantly elevated E/I ratios.

While interesting results regarding E/I imbalance were derived ex-vivo (in humans), studies in-vivo regarding E/I imbalance in AD are lacking, as the activity of excitatory vs. inhibitory neuronal populations cannot be directly measured using neuroimaging. Most works focusing on whole-brain dynamics studied different measures of brain activation patterns, e.g., from its connectivity, but were not informative regarding the role of excitatory vs. inhibitory neuronal populations [18, 19, 20, 21, 22]. To disentangle mechanistic contributions of separate neuronal populations, whole-brain dynamic models can contribute to analyze collective properties of the brain [23, 24, 25], such as the fMRI signal [26, 27, 28, 29]. To understand the complex interplay between pathophysiological processes and brain activity (i.e., the fMRI signal), models might become even more informative when incorporating heterogeneity of brain dynamics in brain regions, based on empirical data [30, 31, 32].

Earlier work specifically on AD using whole-brain simulations focused only on linking global and local brain dynamics to individual differences in cognitive performance scores from different subject conditions [18]. Demirtaş [20] et al. studied the effect of heterogeneity of local synaptic strengths on a large-scale dynamical circuit model of human cortex in healthy subjects, showing that heterogeneity significantly improved the fitting of fMRI resting-state functional connectivity, and was able to capture sensory-association organization of multiple fMRI features. Following this approach, recent work by Stefanovski and co-authors [21] focused on the connection of $A\beta$ with neural function in The Virtual Brain (TVB) platform [33], using a network of interconnected (through the corresponding structural connectivity matrix) Jansen-Rit models [34], addressing the phenomenon of hyperexcitability in AD, examining how $A\beta$ burden modulates regional Excitation-Inhibition balance, leading to local hyperexcitation with high $A\beta$ loads in the model, reproducing what has been previously observed in experimental studies. The resulting simulated local field potentials improved previous diagnostic classifications between AD and controls [22].

However, all these works study the effect of a single burden, namely $A\beta$, on the brain neuronal dynamics, while the work we present here focuses mostly on the *interplay* of both burdens, i.e., $A\beta$ and tau, assessing their relative impacts on these dynamics.

The main objective of this paper is to use whole-brain modeling techniques to study the impact of both $A\beta$ and tau on the dynamics of the regional behaviors in AD. As such, we used our results to discern the impact of each protein in isolation and in combination, being able to assess their relative weights on contributing to abnormal brain activity. We use the Balanced Dynamic Mean Field (BEI) model [31], where local neuronal dynamics of each region evolve according to a dynamic mean field model derived from the behavior of interacting excitatory and inhibitory populations. We will show in this work a clear dominance of the effects of $A\beta$ over tau in the earlier stages of the disease (Mild Cognitive Impairment, MCI), and a dominance of protein tau over the ones of $A\beta$ on the function of the brain dynamics in advanced stages (manifest dementia).

2. Methods Overview

Model Creation: Figure 1a presents an overview of our overall analysis strategy, and the details could be found in the Methods Section. We make use of MRI and positron emission tomography (PET) from the Alzheimer's Disease Neuroimaging Initiative (ADNI). In summary, we use diffusion MRI to generate the structural connectomes of healthy controls (HC), mild cognitive impairment (MCI) and Alzheimer's Disease (AD) subjects. We use task-free resting-state functional MRI to fit a whole-brain model in which the local neuronal dynamics of each brain region evolves according to the dynamic mean field model by Deco et al. [31], which is then connected to a spontaneous blood-oxygenation-level-dependent (BOLD) dynamics. We refer to this model as the *Balanced Excitation-Inhibition (BEI)* model, which can be thought of as a homogeneous reference against which we evaluate the performance of our heterogeneous AD model. $A\beta$ and tau distributions are derived from AV-45 and AV-1451 PET from ADNI. For the heterogeneous model, we incorporate regional heterogeneous distributions of the main proteins involved in AD, namely $A\beta$ and tau, as first order multiplicative polynomials for each burden and for each type of population (excitatory/inhibitory) into the local gain parameter $M_{(E,I)}$. Fitting the model to empirical fMRI data allows us to evaluate which effect of $A\beta$ and tau to the different populations can mechanistically explain the observed behaviors.

Model Fitting: For both of our models, homogeneous and heterogeneous, we assume that all diffusion MRI-reconstructed streamline fibers have the same conductivity and thus the coupling between different brain areas is scaled by a single global parameter, G . We first tune the G parameter of the BEI model to adjust the strength of effective coupling in the model and identify the brain's dynamic working-point by fitting the model to three empirical properties that are estimated from the empirical fMRI data:

- the Pearson correlation between model and empirical estimates of static (i.e., time-averaged) functional connectivity estimated across all pairs of brain regions (FC);
- similarity in sliding-window functional connectivity dynamics (swFCD);
- the KS distance between a set of dynamic functional connectivity matrices (also called coherence connectivity matrix [35]) built from the average BOLD time series of each ROI, which were Hilbert-transformed to yield the phase evolution of the regional signals (phFCD).

We then fit the coefficients for the two burdens, for excitatory and inhibitory populations, with a global optimization algorithm, within directional bounds obtained from previous clinical observations (see below, in Section 5.7).

Result Evaluation: We evaluate the quality of the results in two ways. First, we shuffle the input burdens, and compare the result of performing the simulation with

- the optimized parameters with shuffled burdens.
- the optimized parameters with original (i.e., not shuffled) burdens.
- the homogeneous BEI model.

Second, we examine the relevance of each type of burden by optimizing them in isolation of each other (i.e., zeroing the other one out), and comparing the results. The full comparisons include both burdens in isolation, both burdens simultaneously, and with the homogeneous (i.e., BEI) model. See Figure 1b.

3. Results

We used diffusion MRI to generate a the Structural Connectomes of 17 healthy control (HC) subjects, 9 mild cognitive impairment (MCI) subjects and 10 subjects with Alzheimer's Disease (AD) from ADNI, which are mostly the same participants as used by Stefanovski et al. [21] and Triebkorn et al. [22]. See Table 1.

Diagnosis	n (female)	Mean age	σ	Min. age	Max. age	Mean MMSE	σ_{MMSE}	Min. MMSE	Max. MMSE
AD	10 (5)	72.0	9.6	55.9	86.1	21.3	6.8	9	30
HC	17 (10)	70.8	4.3	63.1	78.0	29.3	0.7	28	30
MCI	9 (3)	68.8	5.8	57.8	76.6	27.4	1.5	25	30

Table 1. Epidemiological information of the population used in this study.

3.1 Fitting the Homogeneous Model

As a first step, we evaluated the capability of the homogeneous BEI model to reproduce empirical properties of resting-state FC data. To this end, we fitted the global coupling parameter, G , without considering heterogeneity by setting all regional gain parameters $M_{(E,I)} = 1$ [36, 31]. Then, we evaluated the ability of the model to reproduce three different properties of empirical resting-state fMRI recordings: edge-level static FC, swFCD, and phFCD (see Methods for further details.) The results of this analysis are shown in Figure 2A. To remove differences across subjects related to age, we considered averaged values across subjects over the healthy control group, and took an equivalent number of simulated trials with the same duration as the human experiments (see Methods). Following previous research [37, 38, 32] fitting the phFCD better captures the spatiotemporal structure of the fMRI data, being a stronger constraint on the model. Indeed, where FC fits are consistently high across a broad range of G values, phFCD yields a clear global optimum at $G = 3.1$. Thus, we choose to use phFCD for all further analysis.

3.2 Introducing $A\beta$ and tau heterogeneity

Once the global coupling parameter has been found, we can introduce the regional heterogeneity in the distributions of $A\beta$ and tau, and study how their introduction leads to a better representation of neural dynamics, i.e., improves the fitting of phFCD. Spatial maps for each form of protein burden used in our modeling are shown in Figures 2G (for $A\beta$) and 2H (for tau) for one particular individual. For some individuals, (mainly HC subjects, e.g., as subject 003_S_6067 in the ADNI database, with $\rho = 0.92$, $p < 0.001$) the $A\beta$ and tau distributions are strongly correlated, while for others the two maps show a weaker correlation (e.g., subject 036_S_4430, with $\rho = 0.10$, $p = 0.04$.) This observation indicates that each protein burden introduces a different form of biological heterogeneity to the benchmark BEI model, and thus should be modeled separately in our simulations.

We introduce these kinds of heterogeneity by modulating the regional gain functions $M_{(E,I)}$ at the optimal working point of the homogeneous BEI model found at the previous stage ($G = 3.1$), through the bias and scaling parameters introduced above, denoted $b_{A\beta}^E$ and $s_{A\beta}^E$ for $A\beta$, and b_{τ}^E and s_{τ}^E for tau, all for the excitatory case, and similarly for the inhibitory case with superscript I . We perform a search in parameter space with constraints introduced from experimental observations, see Section 5.7, to find the optimal working point for the two protein burdens simultaneously, which results in an 8-degree of freedom optimization, which is reduced to six degrees due to the constraints. For the optimization we used **Bayesian optimization algorithm using Gaussian Processes**, see Section 5.10. We can also perform a simplified search, limited to the two-variable $b_{A\beta}^I$ and $s_{A\beta}^I$ space, i.e., the inhibitory bias and scaling of the $A\beta$ influence on inhibitory neuron parameters (Equation 9). In this case, the 2D optimization results show a decreasing the neuronal activity with increasing $A\beta$ concentration, confirming previous results [21]. On average, for each group of subjects, we got the results shown numerically in Table 2.

Cohort	$b_{A\beta}^E$	$s_{A\beta}^E$	b_{τ}^E	s_{τ}^E	$b_{A\beta}^I$	$s_{A\beta}^I$
AD	0.2 (0.5)	2.3 (1.2)	-0.4 (0.6)	-2.6 (0.8)	0.2 (0.6)	-2.5 (0.8)
MCI	0.4 (0.7)	1.7 (1.5)	-0.5 (0.5)	-2.8 (0.7)	-0.1 (0.8)	-2.1 (1.2)
HC	0.1 (0.8)	1.7 (0.9)	-0.5 (0.6)	-2.8 (1.0)	0.3 (0.6)	-3.1 (1.0)

Table 2. Resulting averaged parameters from the optimization procedure. In parenthesis, the respective standard deviations.

These results can be seen visually at Figure 3. This figure shows that there is a clear regime in which all three empirical properties are fitted well by the model, particularly for the values shown above, where a fitting of phFCD of 0.13 is achieved for the AD subjects, while the reference homogeneous value is equal to 0.5.

3.3 Analysis of burden impact

For the optimal parameter values resulting from model fitting, we simulated each dynamical model 10 times for each subject to account for the inherent stochastic nature of the models and compute the respective measures of model fit. Figure 4 shows the distributions of fit statistics across runs for the homogeneous and the heterogeneous model for the different cohorts. In addition, we show results for a null ensemble of models in which the regional burden values were spatially shuffled to generate surrogates with the same spatial autocorrelation as the empirical data. Across the benchmark property to which the data were fitted —phFCD—, the models taking into account the regional burden heterogeneity perform better than the homogeneous

model (all pass the Mann-Whitney U rank test on two *independent samples* with $p < .0005$). We also find a consistent gradient of performance across all benchmarks, with the heterogeneous model performing best, and the homogeneous model showing the poorest performance. For each benchmark metric, the performance of the heterogeneous model was better than all other models (in all cases $p < .06$). Also, it must be noted that the differences in fit statistics between models are significant, as shown in Figure 4. For example, for the AD cohort, the correlation of the median phase FCD between the fitted model and empirical data showed $r < 0.1$ for the heterogeneous model, and $r \approx 0.2$ for the BEI model. In all subject groups, the difference between these two models is clear, with $p < 0.0005$.

Finally, we performed an analysis comparing the impact of each type of burden, in isolation or together, onto the simulation results. In Figures 2D-2F we can see these results for the different cohorts, for $A\beta$ and tau, $A\beta$ alone, tau alone and finally the homogeneous BEI model, added for reference. As we can see, with respect to the homogeneous model, the best performance is systematically obtained by the combined action of both $A\beta$ and tau, giving a value with $p < 0.0004$ in all cases. However, for each cohort, each protein shows to play a different role in the development of the disease. For AD subjects, the effect of $A\beta$ on the optimal combined result is small, with a $p < 0.0005$, while the influence of tau alone has a p value that does not allow us to distinguish between its effect and the combined effect of both proteins ($p = 0.172$), implying a clear dominance of tau over $A\beta$ in this stage of the disease. Also, with respect to the homogeneous BEI model, tau presents $p < 0.005$, while $A\beta$ alone shows a much higher value ($p = 0.339$), not allowing us to clearly distinguish between these two models. In the case of the MCI cohort, in Figure 2E, we can observe that the effect of $A\beta$ alone clearly gives the major contribution to the final combined fitting, rather than tau, with a $p < 0.0003$ between all cases. Finally, in the HC case in Figure 2D, the effects of the $A\beta$ and tau proteins are close to the homogeneous BEI model, with $A\beta$ presenting a somewhat higher prevalence than tau. However, it is noticeable that the differences between this case and the previous one are small, showing that $A\beta$ already plays an important role even in HC subjects.

4. Discussion

In this paper we studied the influence of the regional variability of two pathological proteins, namely $A\beta$ and tau, on cortical activity and E/I balance in the context of AD. The incorporation of such heterogeneous patterns of neuropathology into whole-brain models of neuronal dynamics has been made possible by the availability of in-vivo quantitative PET imaging. We have shown that the heterogeneous model incorporating both types of neuropathological burdens more faithfully reproduces empirical properties of dynamic FC than the standard model with fixed and homogeneous parameters. Our findings highlight a central role of both types of burden on the regional neuronal dynamics in AD, supporting the hypothesis of hyper excitation in AD, and the crucial role of E/I balance. Regarding their influence on brain activity, our results have shown a dominance of $A\beta$ influence on neural dynamics in earlier stages of AD (i.e., MCI) and even in healthy controls, while the tau influence plays a larger role in later stages. These key findings highlight their prominent role in contributing to the abnormal brain activity patterns in the course of AD [39].

4.1 How does burden heterogeneity shape neuronal dynamics?

We introduced burden heterogeneity into our dynamical model by modifying the regional excitability of local population activity. We achieved this by modifying each region's gain response function M_i of inhibitory and excitatory populations, in accordance with previous works exploring the effect of regional parameters on E/I balance [32], thus focusing on how the interaction of neuronal populations contributes to neuronal dynamics (i.e., FC or FCD) and their relative impacts over time. Our approach is different from the work by Stefanovski et al. [21], where the $A\beta$ burden was used to modulate regional E/I balance by negatively modulating the inhibitory time constant, increasing excitatory activity and producing a higher output of the pyramidal cell populations, resulting in a local hyperexcitation with high $A\beta$ loads. However, as seen in Methods, our results confirm their findings with respect to the behavior of the $A\beta$ burden in early stages of the disease, resulting in a net increase of the excitatory activity with increased $A\beta$ burden. There are other approaches available to introduce heterogeneity, such as an adjustment of the inter-node connectivity to fit empirical and simulated FCs [40]; or variations of within- and inter-area connectivity [41]. However, based on the empirical evidence that the interplay of both burdens, $A\beta$ and tau, severely disrupt normal neuronal function, we decided to model their direct effect on the E/I balance.

In this paper we have chosen to incorporate heterogeneity into the model by modulating population gain response functions $H^{(E,I)}$, since local variations in the E/I balance will affect the net excitability of the population, which in turn is captured by the gain function parameter, M_i . We thus assume that changes in regional gain are the common final pathways of different neuropathology-related pathomechanisms which might have an influence on specific neuronal populations or interaction between populations.

In particular, we introduced regional variations of M_i as the product of linear terms consisting of a constant (bias), and a scaling factor. This introduced eight degrees of freedom, which we could narrow down to six due to constraints based on previous literature [11], which helped to considerably reduce the search space. In sum, our model was created based

the assumptions that $A\beta$ leads to GABAergic interneuron dysfunction and impaired glutamate reuptake, while tau leads to reduced synaptic neurotransmitter release in excitatory cells. This amount of degrees is substantially less than used in other models [41, 40], making a fast parameter optimization feasible. For the optimization we used Bayesian optimization using Gaussian Processes (see Methods), because of the many minima that could trap traditional optimization methods.

4.2 Evaluating $A\beta$ and tau impact

A large body of scientific literature focused on linking global and local brain dynamics to individual differences in cognitive performance scores [18], showing that patients with AD and MCI show less variation in neuronal connectivity during resting-state [42], and even presented benchmarks for predictive models for resting-state fMRI, revealing biomarkers of individual psychological or clinical traits [19]. However, the pattern of neuronal connectivity alterations has been incompletely understood. More recent work focus on the effect of $A\beta$ on hyperexcitability, addressing the fact that this protein modulates regional E/I balance, resulting in local hyperexcitation with high loads [21]. To our knowledge, no prior study has evaluated both types of neuropathological burden, $A\beta$ and tau, simultaneously.

As explained in Methods, we compared the impact of each type of burden, in isolation or interacting, onto neural dynamics. We found that the model fitting optimum is systematically obtained by the interaction of both burdens. Also, we have found that for each condition (i.e., HC, MCI or AD), each protein has a different impact on the disease. In the case of AD, $A\beta$ has a small impact on the combined result, while tau alone had almost all of the impact, showing its dominance over $A\beta$. Also, in comparison to the homogeneous BEI model, in we observed that tau is clearly distinguishable, but $A\beta$ is not. Taken together, these results imply that we cannot distinguish between the effect on brain activity of both proteins together vs. the effect of tau alone, while the effect of $A\beta$ is clearly distinguishable from the combined effect. As a consequence, this allows us to conclude that the impact of tau in this stage (AD) of the disease is clearly dominant over $A\beta$. In MCI, the influence of $A\beta$ alone is clearly dominant over tau, see Figure 2E. Finally, when studying the effect of both proteins in the HC case, we can observe that the effect of the $A\beta$ and tau proteins is close to the homogeneous BEI model, with $A\beta$ presenting a relatively higher influence than tau. The influence of $A\beta$ both in MCI patients as well as in HC shows that $A\beta$ leads to a measurable change in brain dynamics, independent of existing cognitive impairment, in elderly subjects. Despite our findings from model fitting, we acknowledge that we only observe the current influence of $A\beta$ vs. tau in different disease stages in a cross-sectional cohort. Longitudinal examinations might also replicate the abundant evidence in the literature [11] that both proteins interplay a toxic feedback loop which is the ultimate responsible (perhaps among other factors) of the development of the disease.

Our analysis shows that edge-level measures of static FC offer loose constraints for model optimization, showing comparably high fit statistics across a broad range of values of the global coupling parameter. In contrast, fitting to dynamical functional connectivity shows a clear optimum, mirroring similar results reported previously [43, 32]. We can conclude that fitting models to both static and dynamic properties is thus important for identifying an appropriate working point for each model.

Across all these properties, we observe that the model that incorporates the heterogeneous burden loads provides a better match to the data than the homogeneous BEI model, which does not incorporate a fitting of the gain response function of inhibitory and excitatory populations to the data. This shows that constraining regional heterogeneity by the protein burdens yields a more faithful replication of empirical pHCD. The superiority of our model using heterogeneous, empirically estimated parameters, suggests that regional heterogeneity plays a significant role in shaping the effects of Alzheimer's disease on spontaneous BOLD-dynamics. However, as we already mentioned, it must be noted that the differences in fit statistics between models are significant. These results suggest that these empirical fit statistics have good capacity to tease apart dynamical differences between models, which gives the opportunity to disentangle the influence of different pathomechanisms in vivo.

We observe that, in all cases, the bias parameters for the different burdens (Figure 3) are approximately 0 in all cases, thus indicating that the influence of the bias parameters with respect to the homogeneous model can be ignored, reducing computational complexity. The respective scaling parameters take non negligible values, showing a linear relationship between $A\beta$ and tau on neural dynamics. In our model, in earlier stages of the disease (i.e., MCI) $A\beta$ has a higher scaling parameter than tau, suggesting a higher contribution to the E/I imbalance. In later stages, we observe the opposite, which might indicate that tau burden is more closely related to neuronal dysfunction in these stages, which replicates our results regarding the model fitting using different types of heterogeneous models. We acknowledge that on a pathophysiological level there is a strong interplay between $A\beta$ and tau and further (causal) research is needed to clearly discern the role each protein plays in the generation of neuronal dysfunction.

In summary, in this paper we have presented a whole-brain computational model connecting the main protein burdens, namely $A\beta$ and tau, with the different stages of AD and in HC. The results we obtained not only reproduce previous research regarding E/I imbalance in AD, but also shed further light on the relative impact of each type of burden during different disease stages, opening new avenues to focus research efforts. As a general conclusion, our study shows that whole-brain modeling enables research on disease mechanisms in-vivo, demonstrating its potential to produce improved diagnostics and help in the discovery of new treatments.

5. Methods

5.1 Participants

Empirical data were obtained from the Alzheimer's Disease Neuroimaging Initiative (ADNI) database (adni.loni.usc.edu), which is a longitudinal multi-site study designed to develop biomarkers for Alzheimer's disease (AD) across all stages. The inclusion criteria for AD patients was the NINCDS-ADRDA criteria, which contains only clinical features [4], and a MMSE score below 24. For both HC and MCI, the inclusion criteria were a MMSE (Mini Mental State Examination) score between 24-30, as well as age between 55-90 years. Also, for MCI, participants had to have a subjective memory complaint and abnormal results in another neuropsychological memory test. Imaging and biomarkers were not used for the diagnosis.

5.2 Data Acquisition and Processing

All the data in this study were previously used in Stefanovski et al. [21] work, so we will present here an abridged version of the processing performed on the original data and refer to the original work for the details. All images used in this study were taken from ADNI-3, using data from Siemens scanners with a magnetic field strength of 3T.

5.2.1 Structural MRI

For each included participant, we created a brain parcellation for our structural data using FLAIR, following the minimal preprocessing pipeline [44] of the Human Connectome Project (HCP) using Freesurfer¹ [45], FSL [46, 47, 48] and connectome workbench². Therefore, we used T1 MPRAGE, FLAIR and fieldmaps for the anatomical parcellation. We then registered the subject cortical surfaces to the parcellation of Glasser et al. [49] using the multimodal surface matching (MSM) tool [50]. In this parcellation, there were 379 regions: 180 left and 180 right cortical regions, 9 left and 9 right subcortical regions, and 1 brainstem region.

5.2.2 PET Images

For $A\beta$, we used the version of AV-45 PET already preprocessed by ADNI, using a standard image with a resolution of 1.5mm cubic voxels and matrix size of $160 \times 160 \times 96$, normalized so that the average voxel intensity was 1 and smoothed out using a scanner-specific filter function. Then, a brainmask was generated from the structural preprocessing pipeline (HCP) and used to mask the PET image. On the other hand, to obtain the local burden of $A\beta$, we computed the relative intensity to the cerebellum. We received in each voxel a relative $A\beta$ burden which is aggregated according to the parcellation used for our modeling approach. Subcortical region PET loads were defined as the average SUVR in subcortical gray matter (GM). With the help of the connectome workbench tool, using the pial and white matter surfaces as ribbon constraints, we mapped the Cortical GM PET intensities onto individual cortical surfaces. Finally, using the multimodal Glasser parcellation we derived average regional PET loads.

For tau, we also used ADNI's preprocessed version of AV-1451 (Flortaucipir) following the same acquisition and processing, resulting in a single relative tau value for each voxel. Then, these values were also aggregated to the selected parcellation, also following the already mentioned steps. The final average regional tau loads were obtained in the Glasser parcellation.

5.2.3 DWI

Individual tractographies were computed only for included HC participants, and they were averaged to a standard brain template (see below). Preprocessing was mainly done with the MRtrix3 software package³.

In particular, the following steps were performed: First, we denoised the DWI data [51], followed by motion and eddy current correction⁴. Then, B1 field inhomogeneity correction (ANTS N4), followed by a brainmask estimation from the DWI images. Next, we normalized the DWI intensity for the group of participants, which was used to generate a WM response function [52], and created an average response function from all participants. Next, we estimated the fiber orientation distribution and the average response function [53] using the subject normalized DWI image, to finally generate a five tissue type image. Finally, we used the iFOD2 algorithm [54] and the SIFT2 algorithm [55] to get the weighted anatomical constrained tractography [56], to end up merging all information into the Glasser connectome, resulting in a structural connectome (SC).

5.2.4 fMRI

With respect to the processing of the fMRI data, the images were initially preprocessed in FSL FEAT and independent component analysis-based denoising (FSLFIX) following a basic pipeline [21]. Time courses for noise-labeled components, along with 24 head motion parameters, were then removed from the voxel-wise fMRI time series using ordinary least squares regression.

¹<https://surfer.nmr.mgh.harvard.edu/fswiki/FreeSurferMethodsCitation>

²<https://www.humanconnectome.org/software/connectome-workbench>

³<http://www.mrtrix.org>

⁴https://mrtrix.readthedocs.io/en/latest/dwi_preprocessing/dwipreproc.html

The resulting denoised functional data were spatially normalized to the MNI space using Advanced Normalization Tools (version 2.2.0). Mean time series for each parcellated region were then extracted, and interregional FC matrices were estimated using Pearson correlations between each pair of regional time series. Dynamic FC matrices were also calculated for the empirical data, as outlined below.

5.3 Generation of a Standard Brain Template

As previously done [21], we average the SCs of all HC participants, using an arithmetic mean

$$C_{\mu} = (\sum_{i=1}^n C_i) / n = (C_1 + C_2 + \dots + C_n) / n$$

wherein C_{μ} is the averaged SC matrix, n is the number of HC participants and C_i is the individual SC matrix.

However, as matrices in this context are large (i.e., 379 regions), the average input to any given node can be too large for the DMF, making fitting and processing in general more difficult. Thus, we discarded the traditional normalization of dividing the matrix elements by its maximum, and used a slightly different approach, instead. First, we added one and applied the logarithm to every entry, as $IC = \log(C_{\mu} + 1)$. Then, we computed the maximum input any node could receive for a unitary unit input current, $maxNodeInput = \max_j(\sum_i(IC_{i,j}))$, and finally we normalized by $0.7 * IC / maxNodeInput$, where 0.7 was chosen to be a convenient normalization value. Observe that this constant is actually multiplying another constant G in the model which we fit to empirical data, so its actual value can safely be changed.

In Figure 5 we can find the SC matrix and organization graph, where we can observe that the general characteristics of physiological SCs such as symmetry, laterality, homology, and subcortical hubs are maintained in the averaged connectome. The election of the averaged SC allowed to control all factors (e.g., atrophy), which matched our objective of simulating the activity from both healthy and “pathogenic” modifications by $A\beta$ and tau.

5.4 Balanced Excitation-Inhibition (BEI) model

In this work we used the Dynamic Mean Field (DMF) model proposed by Deco et al. [31], which consists of a network model to simulate spontaneous brain activity at the whole-brain level. In this model, each node represents a brain area and the links represent the white matter connections between them. In turn, each node is a reduced representation of large ensembles of interconnected excitatory and inhibitory integrate-and-fire spiking neurons (80% and 20% neurons, respectively), to a set of dynamical equations describing the activity of coupled excitatory (E) and inhibitory (I) pools of neurons, based on the original reduction of Wong and Wang [58]. In the DMF model, excitatory synaptic currents, $I(E)$, are mediated by NMDA receptors, while inhibitory currents, $I(I)$, are mediated by $GABA_A$ receptors. Both neuronal pools are reciprocally connected, and the inter-area interactions occur at the excitatory level only, scaled by the structural connectivity C_{kj} (see Section 5.2.1).

To be more specific, the DMF model is expressed by the following system of coupled differential equations:

$$I_k^{(E)} = W_E I_o + w_+ J_N S_k^{(E)} + J_N G \sum_j C_{kj} S_j^{(E)} - J_k S_k^{(I)} + I_{ext} \quad (1)$$

$$I_k^{(I)} = W_I I_o + J_N S_k^{(E)} - S_k^{(I)} + \lambda J_N G \sum_j C_{kj} S_j^{(E)} \quad (2)$$

$$r_k^{(E)} = H^{(E)}(I_k^{(E)}) = \frac{M_k^E(a_E I_k^{(E)} - b_E)}{1 - \exp(-d_E M_k^E(a_E I_k^{(E)} - b_E))} \quad (3)$$

$$r_k^{(I)} = H^{(I)}(I_k^{(I)}) = \frac{M_k^I(a_I I_k^{(I)} - b_I)}{1 - \exp(-d_I M_k^I(a_I I_k^{(I)} - b_I))} \quad (4)$$

$$\dot{S}_k^{(E)} = -\frac{S_k^{(E)}}{\tau_E} + (1 - S_k^{(E)}) \gamma H^{(E)}(I_k^{(E)}) \quad (5)$$

$$\dot{S}_k^{(I)} = -\frac{S_k^{(I)}}{\tau_I} + H^{(I)}(I_k^{(I)}) \quad (6)$$

Here, the last *two* equations should add, when integrating, an uncorrelated standard Gaussian noise term with an amplitude of $\sigma = 0.01nA$ (using Euler-Maruyama integration). In these equations, λ is a parameter that can be equal to 1 or 0, indicating whether long-range feedforward inhibition is considered ($\lambda = 1$) or not ($\lambda = 0$).

As mentioned, the DMF model is derived from the original Wong and Wang model [58] to emulate resting-state conditions, such that each isolated node displays the typical noisy spontaneous activity with low firing rate ($H^{(E)} \sim 3Hz$) observed in electrophysiology experiments, reusing most of the parameter values defined there. We also implemented the Feedback Inhibition Control (FIC) mechanism described by Deco et al. [31], where the inhibition weight, J_n , was adjusted separately for each node n such that the firing rate of the excitatory pools $H^{(E)}$ remains clamped at 3Hz even when receiving excitatory input from connected areas. Deco et al. [31] demonstrated that this mechanism leads to a better prediction of the resting-state FC and to a more realistic evoked activity. We refer to this model as the balanced excitation-inhibition (BEI) model. Although the local adjustments in this model introduce some degree of regional heterogeneity, the firing rates are constrained to be uniform across regions so we consider this BEI model as a homogeneous benchmark against which we evaluate more sophisticated models that allow $A\beta$ and tau to affect intrinsic dynamical properties across regions.

Following the Glasser parcellation [44], we considered $N = 379$ brain areas in our whole-brain network model. Each area n receives excitatory input from all structurally connected areas into its excitatory pool, weighted by the connectivity matrix, obtained from dMRI (see Section 5.2.3). Furthermore, all inter-area E-to-E connections are equally scaled by a global coupling factor G . This global scaling factor is the only control parameter that is adjusted to move the system to its optimal working point, where the simulated activity maximally fits the empirical resting-state activity of healthy control participants. Simulations were run for a range of G between 0 and 5.5 with an increment of 0.05 and with a time step of 1 ms. For each G , we ran 200 simulations of 435 s each, in order to emulate the empirical resting-state scans from 17 participants. The optimum value found, for the *phFCD* observable, is for $G = 3.1$. See Figure 2A.

5.5 Simulated BOLD signal

Once we have obtained the simulated mean field activity, we need to transform it into a BOLD signal we used the generalized hemodynamic model of Stephan et al. [59]. We compute the BOLD signal in the k -th brain area from the firing rate of the excitatory pools $H^{(E)}$, such that an increase in the firing rate causes an increase in a vasodilatory signal, s_k , that is subject to auto-regulatory feedback. Blood inflow f_k responds in proportion to this signal inducing changes in blood volume v_k and deoxyhemoglobin content q_k . The equations relating these biophysical variables are:

$$\begin{aligned} \frac{ds_k}{dt} &= 0.5r_k^{(E)} + 3 - ks_k - \gamma(f_k - 1) \\ \frac{df_k}{dt} &= s_k \\ \tau \frac{dv_k}{dt} &= f_k - v_k^{\alpha-1} \\ \tau \frac{dq_k}{dt} &= f_k \frac{1 - (1 - \rho)^{f_k}}{\rho} - q_k \frac{v_k^{\alpha-1}}{v_k} \end{aligned} \tag{7}$$

with finally

$$B_k = v_0 \left[k_1(1 - q_k) + k_2(1 - \frac{q_k}{v_k}) + k_3(1 - v_k) \right]$$

being the final measured BOLD signal.

We actually used the updated version described later on [59], which consists on introducing the change of variables $\hat{z} = \ln z$, which induces the following change for $z = f_k, v_k$ and q_k , with its corresponding state equation $\frac{d\hat{z}}{dt} = F(\hat{z})$, as:

$$\frac{d\hat{z}}{dt} = \frac{d \ln(z)}{dz} \frac{dz}{dt} = \frac{F(z)}{z}$$

which results in $z(t) = \exp(\hat{z}(t))$ always being positive, which guarantees a proper support for these non-negative states, and thus numerical stability when evaluating the state equations during evaluation.

5.6 $A\beta$ -Tau model:

In our heterogeneous model, $A\beta$ and Tau are introduced, at the formulae for the neuronal response functions, $H^{(E,I)}$ (excitatory/inhibitory), into the gain factor $M_k^{(E,I)}$ for the k -th area as

$$M_k^E = (1 + b_{A\beta}^E + s_{A\beta}^E A\beta_k)(1 + b_\tau^E + s_\tau^E \tau_{auk}) \tag{8}$$

$$M_k^I = (1 + b_{A\beta}^I + s_{A\beta}^I A\beta_k)(1 + b_\tau^I + s_\tau^I \tau_k) \quad (9)$$

where $b_{(A\beta, \tau)}^{(E, I)}$ are the excitatory/inhibitory $A\beta$ and tau bias parameters, while $s_{(A\beta, \tau)}^{(E, I)}$ are the respective scaling factors. These are the 8 (from which actually only 6 are needed as tau only affects excitatory neurons [60], see next section) parameters that we will optimize for each subject individually.

5.7 Constraints

Based on previous neuroscientific experiments [11], we included constraints on the direction of effect of $A\beta$ and tau (i.e., inhibitory vs. excitatory influence). We introduced the following constraints:

- $A\beta$ produces inhibitory GABAergic interneuron dysfunction [61, 62], thus we can infer that $s_{A\beta}^I < 0$.
- $A\beta$ produces impaired glutamate reuptake [61, 62], so we can introduce the bound $s_{A\beta}^E > 0$.
- Tau appears to target excitatory neurons [60], so we can safely consider that $b_\tau^I = s_\tau^I = 0$.
- Tau binds to synaptogyrin-3, reducing excitatory synaptic neurotransmitter release [63], thus $s_\tau^E < 0$.

Although the interplay between $A\beta$ and tau is not completely known [11], but there is evidence that $A\beta$ promotes tau by cross-seeding [64, 65], thus the cross term factors (i.e., the ones resulting from the multiplication of $A\beta$ and tau scaling parameters) play a crucial role to elucidate the final impact of the combined burden.

5.8 Observables

edge-centric FC The static edge-level FC is defined as the $N \times N$ matrix of BOLD signal correlations between brain areas computed over the entire recording period (see Figure 5). We computed the empirical FC for each human participant and for each simulated trial, as well as for the group-averages SC matrix of the healthy cohort. All empirical and simulated FC matrices were compared by computing the Pearson correlation between their upper triangular elements (given that the FC matrices are symmetric).

swFCD The most common and straightforward approach to investigate the temporal evolution of FC is the sliding-window FC dynamics (swFCD) [66, 67, 68, 69, 70, 43]. This is achieved by calculating the correlation matrix, $FC(t)$, restricted to a given time-window ($t - x : t + x$), and successively shifting this window in time resulting in a time-varying $FC_{N \times N \times T}$ matrix (where N is the number of brain areas and T the number of time windows considered). Here, we computed the FC over a sliding window of 30 TRs (corresponding approximately to 1.5 minutes) with incremental shifts of 3 TRs. This FCD matrix is defined so that each entry, $(FCD(t_x, t_y))$ corresponds to the correlation between the FC centered at times t_x and the FC centered at t_y . In order to compare quantitatively the spatio-temporal dynamical characteristics between empirical data and model simulations, we generate the distributions of the upper triangular elements of the FCD matrices over all participants as well as of the FCD matrices obtained from all simulated trials for a given parameter setting. The similarity between the empirical and model FCD distributions is then compared using the KS distance, D_{KS} , allowing for a meaningful evaluation of model performance in predicting the changes observed in dynamic resting-state FC. However, the fundamental nature of the swFCD technique implies the choice of a fixed window length, which limits the analysis to the frequency range below the window period, so the ideal window length to use remains under debate [71, 72, 73, 74, 75].

phFCD In an attempt to overcome the limitations of the sliding-window analysis, a few methods were proposed to estimate the $FC(t)$ at the instantaneous level. For instance, phase Functional Connectivity Dynamics (*phFCD*) consists in computing the phase coherence between time series at each recording frame [76, 77, 78, 35]. In brief, the instantaneous BOLD phase of area n at time t , $\theta_n(t)$, is estimated using the Hilbert transform. Given the phase, the angle between two BOLD signals is given by their absolute phase difference: $\Theta_{np} = |\theta_n(t) - \theta_p(t)|$. Then, the $phFCD(t)$ between a pair of brain areas n and p is calculated as:

$$phFCD_{np}(t) = \cos(\Theta_{np}(t)), n, p \in N = 1, \dots, N$$

with N the number of brain regions considered in the parcellation used.

5.9 2D $A\beta$ Optimization

We can use our model to verify the results by Stefanovski et al. [21] by limiting our analysis to the parameters of $A\beta$ at the inhibitory level (i.e., the inhibitory bias $b'_{A\beta}$ and scaling $s'_{A\beta}$ parameters only, defined in Equation 9). This way, we can replicate, up to a certain degree, the results from that paper, being limited by the fact that we use a different model, based on the BEI model instead of the Jansen-Rit model [34]; a different expression for the burden, i.e., a linear approximation instead of a sigmoid; different units, etc. See Figure 3. By analyzing the obtained data at the optimal fit, the same behavior of decreasing the neuronal activity of inhibitory neurons with the scaling parameter $s'_{A\beta}$, corresponding to an increase in $A\beta$ concentration, can be observed, as shown in Figure 6.

5.10 Full Optimization

To efficiently optimize the 6-dimensional function described before for the three bias and scaling values, we used a Bayesian optimization algorithm using Gaussian Processes (GP), which approximates the function using a multivariate Gaussian. In particular, our implementation uses the *gp_optimize* method from the *scikit-optimize* Python library, which uses a GP kernel between the parameters to obtain the covariance of the function values. With this information, the algorithm chooses the next parameter to evaluate by selecting the acquisition function over the Gaussian prior.

Data and code availability statement

All code for implementing computational models and reproducing our results is available at <https://github.com/dagush/WholeBrain>

CRedit authorship contribution statement

Gustavo Patow: Conceptualization, Formal analysis, Software, Writing – original draft, Writing – review & editing. **Leon Stefanovski:** Data Curation, Writing – review & editing. **Petra Ritter:** Data Curation, Writing – review & editing. **Gustavo Deco:** Conceptualization, Writing – review & editing. **Xenia Kobeleva:** Conceptualization, Writing – review & editing.

Declaration of Competing Interest

The authors declare that they have no known competing financial interests or personal relationships that could have appeared to influence the work reported in this paper.

Funding

This research was partially funded by grant PID2021-122136OB-C22 from the Ministerio de Ciencia e Innovación, Spain of GP. This work was supported by an add-on fellowship of the Joachim Herz Foundation of XK. PR had the support of the following grants: H2020 Research and Innovation Action Grant Human Brain Project SGA2 785907 (PR), H2020 Research and Innovation Action Grant Human Brain Project SGA3 945539 (PR), H2020 Research and Innovation Action Grant Interactive Computing E-Infrastructure for the Human Brain Project ICEI 800858 (PR), H2020 Research and Innovation Action Grant EOSC VirtualBrainCloud 826421 (PR), H2020 Research and Innovation Action Grant AISN 101057655 (PR), H2020 Research Infrastructures Grant EBRAINS-PREP 101079717 (PR), H2020 European Innovation Council PHRASE 101058240 (PR), H2020 Research Infrastructures Grant EBRAIN-Health 101058516 (PR), H2020 European Research Council Grant ERC BrainModes 683049 (PR), JPND ERA PerMed PatternCog 2522FSB904 (PR), Berlin Institute of Health & Foundation Charité (PR), Johanna Quandt Excellence Initiative (PR), German Research Foundation SFB 1436 (project ID 425899996) (PR), German Research Foundation SFB 1315 (project ID 327654276) (PR), German Research Foundation SFB 936 (project ID 178316478) (PR), German Research Foundation SFB-TRR 295 (project ID 424778381) (PR), German Research Foundation SPP Computational Connectomics RI 2073/6-1, RI 2073/10-2, RI 2073/9-1 (PR).

Acknowledgements

Data collection and sharing for this project was funded by the Alzheimer's Disease Neuroimaging Initiative (ADNI) (National Institutes of Health Grant U01 AG024904) and DOD ADNI (Department of Defense award number W81XWH-12-2-0012). ADNI is funded by the National Institute on Aging, the National Institute of Biomedical Imaging and Bioengineering, and through generous contributions from the following: AbbVie, Alzheimer's Association; Alzheimer's Drug Discovery Foundation; Araclon Biotech; BioClinica, Inc.; Biogen; Bristol-Myers Squibb Company; CereSpir, Inc.; Cogstate; Eisai Inc.; Elan Pharmaceuticals, Inc.; Eli Lilly and Company; EuroImmun; F. Hoffmann-La Roche Ltd and its affiliated company

Genentech, Inc.; Fujirebio; GE Healthcare; IXICO Ltd.; Janssen Alzheimer Immunotherapy Research & Development, LLC.; Johnson & Johnson Pharmaceutical Research & Development LLC.; Lumosity; Lundbeck; Merck & Co., Inc.; Meso Scale Diagnostics, LLC.; NeuroRx Research; Neurotrack Technologies; Novartis Pharmaceuticals Corporation; Pfizer Inc.; Piramal Imaging; Servier; Takeda Pharmaceutical Company; and Transition Therapeutics. The Canadian Institutes of Health Research is providing funds to support ADNI clinical sites in Canada. Private sector contributions are facilitated by the Foundation for the National Institutes of Health (www.fnih.org). The grantee organization is the Northern California Institute for Research and Education, and the study is coordinated by the Alzheimer's Therapeutic Research Institute at the University of Southern California. ADNI data are disseminated by the Laboratory for Neuro Imaging at the University of Southern California.

References

- [1] H. Braak and E. Braak. Neuropathological staging of alzheimer-related changes. *Acta Neuropathologica*, 82(4):239–259, sep 1991.
- [2] G.L. Wenk. Neuropathologic changes in alzheimer's disease: potential targets for treatment. *J Clin Psychiatry*, 67(3):3–7, 2006.
- [3] Colin L. Masters, Randall Bateman, Kaj Blennow, Christopher C. Rowe, Reisa A. Sperling, and Jeffrey L. Cummings. Alzheimer's disease. *Nature Reviews Disease Primers*, 1(1), October 2015.
- [4] G. McKhann, D. Drachman, M. Folstein, R. Katzman, D. Price, and E. M. Stadlan. Clinical diagnosis of alzheimer's disease: Report of the NINCDS-ADRDA work group under the auspices of department of health and human services task force on alzheimer's disease. *Neurology*, 34(7):939–939, July 1984.
- [5] Leon Stefanovski, Jil Mona Meier, Roopa Kalsank Pai, Paul Triebkorn, Tristram Lett, Leon Martin, Konstantin Bülow, Martin Hofmann-Apitius, Ana Solodkin, Anthony Randal McIntosh, and Petra Ritter. Bridging scales in alzheimer's disease: Biological framework for brain simulation with the virtual brain. *Frontiers in Neuroinformatics*, 15, April 2021.
- [6] Clifford R. Jack, David A. Bennett, Kaj Blennow, Maria C. Carrillo, Billy Dunn, Samantha Budd Haeberlein, David M. Holtzman, William Jagust, Frank Jessen, Jason Karlawish, Enchi Liu, Jose Luis Molinuevo, Thomas Montine, Creighton Phelps, Katherine P. Rankin, Christopher C. Rowe, Philip Scheltens, Eric Siemers, Heather M. Snyder, Reisa Sperling, Cerise Elliott, Eliezer Masliah, Laurie Ryan, and Nina Silverberg. NIA-AA research framework: Toward a biological definition of alzheimer's disease. *Alzheimer's & Dementia*, 14(4):535–562, April 2018.
- [7] Johannes Weickenmeier, Ellen Kuhl, and Alain Goriely. Multiphysics of prionlike diseases: Progression and atrophy. *Phys. Rev. Lett.*, 121:158101, Oct 2018.
- [8] G. Caleb Alexander and Jason Karlawish. The problem of aducanumab for the treatment of alzheimer disease. *Annals of Internal Medicine*, 174(9):1303–1304, sep 2021.
- [9] Lars M. Ittner and Jürgen Götz. Amyloid- β and tau — a toxic pas de deux in alzheimer's disease. *Nature Reviews Neuroscience*, 12(2):67–72, December 2010.
- [10] Margaret Lock. *The Alzheimer conundrum : entanglements of dementia and aging*. Princeton University Press, Princeton, 2013.
- [11] Marc Aurel Busche and Bradley T. Hyman. Synergy between amyloid- β and tau in alzheimer's disease. *Nature Neuroscience*, 23(10):1183–1193, August 2020.
- [12] Eva Vico Varela, Guillaume Etter, and Sylvain Williams. Excitatory-inhibitory imbalance in alzheimer's disease and therapeutic significance. *Neurobiology of Disease*, 127:605–615, July 2019.
- [13] Fernando Maestú, Willem de Haan, Marc Aurel Busche, and Javier DeFelipe. Neuronal excitation/inhibition imbalance: core element of a translational perspective on alzheimer pathophysiology. *Ageing Research Reviews*, 69:101372, August 2021.
- [14] Che-Wei Chang, Mark D. Evans, Xinxing Yu, Gui-Qiu Yu, and Lennart Mucke. Tau reduction affects excitatory and inhibitory neurons differently, reduces excitation/inhibition ratios, and counteracts network hypersynchrony. *Cell Reports*, 37(3):109855, October 2021.
- [15] Danlei Bi, Lang Wen, Zujun Wu, and Yong Shen. GABAergic dysfunction in excitatory and inhibitory (e/i) imbalance drives the pathogenesis of alzheimer's disease. *Alzheimer's & Dementia*, 16(9):1312–1329, June 2020.
- [16] Alexandra L Petrache, Aarib Rajulawalla, Anqi Shi, Andrea Wetzel, Takashi Saito, Takaomi C Saido, Kirsten Harvey, and Afia B Ali. Aberrant excitatory-inhibitory synaptic mechanisms in entorhinal cortex microcircuits during the pathogenesis of alzheimer's disease. *Cerebral Cortex*, 29(4):1834–1850, February 2019.

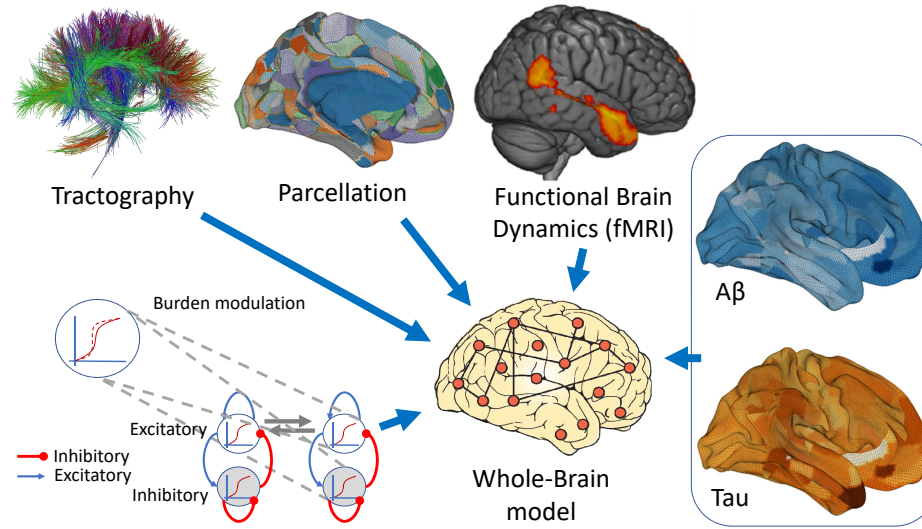
- [17] Julie C. Lauterborn, Pietro Scaduto, Conor D. Cox, Anton Schulmann, Gary Lynch, Christine M. Gall, C. Dirk Keene, and Agenor Limon. Increased excitatory to inhibitory synaptic ratio in parietal cortex samples from individuals with alzheimer's disease. *Nature Communications*, 12(1), May 2021.
- [18] J. Zimmermann, A. Perry, M. Breakspear, M. Schirner, P. Sachdev, W. Wen, N.A. Kochan, M. Mapstone, P. Ritter, A.R. McIntosh, and A. Solodkin. Differentiation of alzheimer's disease based on local and global parameters in personalized virtual brain models. *NeuroImage: Clinical*, 19:240 – 251, 2018.
- [19] Kamalaker Dadi, Mehdi Rahim, Alexandre Abraham, Darya Chyzyk, Michael Milham, Bertrand Thirion, and Gaël Varoquaux. Benchmarking functional connectome-based predictive models for resting-state fmri. *NeuroImage*, 192:115 – 134, 2019.
- [20] Murat Demirtaş, Joshua B. Burt, Markus Helmer, Jie Lisa Ji, Brendan D. Adkinson, Matthew F. Glasser, David C. Van Essen, Stamatis N. Sotiropoulos, Alan Anticevic, and John D. Murray. Hierarchical heterogeneity across human cortex shapes large-scale neural dynamics. *Neuron*, 101(6):1181–1194.e13, March 2019.
- [21] Leon Stefanovski, Paul Triebkorn, Andreas Spiegler, Margarita-Arimatea Diaz-Cortes, Ana Solodkin, Viktor Jirsa, Anthony Randal McIntosh, Petra Ritter, and for the Alzheimer's Disease Neuroimaging Initiative . Linking molecular pathways and large-scale computational modeling to assess candidate disease mechanisms and pharmacodynamics in alzheimer's disease. *Frontiers in Computational Neuroscience*, 13:54, 2019.
- [22] Paul Triebkorn, Leon Stefanovski, Kiret Dhindsa, Margarita-Arimatea Diaz-Cortes, Patrik Bey, Konstantin Bülow, Roopa Pai, Andreas Spiegler, Ana Solodkin, Viktor Jirsa, Anthony Randal McIntosh, and Petra Ritter and. Brain simulation augments machine-learning-based classification of dementia. *Alzheimer's & Dementia: Translational Research & Clinical Interventions*, 8(1), January 2022.
- [23] Gustavo Deco and Morten L. Kringelbach. Great expectations: Using whole-brain computational connectomics for understanding neuropsychiatric disorders. *Neuron*, 84(5):892–905, December 2014.
- [24] Matthieu Gilson, Nikos E. Kouvaris, Gustavo Deco, Jean-François Mangin, Cyril Poupon, Sandrine Lefranc, Denis Rivière, and Gorka Zamora-López. Network analysis of whole-brain fMRI dynamics: A new framework based on dynamic communicability. *NeuroImage*, 201:116007, November 2019.
- [25] Morten L. Kringelbach and Gustavo Deco. Brain states and transitions: Insights from computational neuroscience. *Cell Reports*, 32(10):108128, September 2020.
- [26] Anandamohan Ghosh, Y. Rho, A. R. McIntosh, R. Kötter, and V. K. Jirsa. Noise during rest enables the exploration of the brain's dynamic repertoire. *PLoS Computational Biology*, 4(10):e1000196, October 2008.
- [27] G. Deco, V. Jirsa, A. R. McIntosh, O. Sporns, and R. Kötter. Key role of coupling, delay, and noise in resting brain fluctuations. *Proceedings of the National Academy of Sciences*, 106(25):10302–10307, June 2009.
- [28] C. J. Honey, O. Sporns, L. Cammoun, X. Gigandet, J. P. Thiran, R. Meuli, and P. Hagmann. Predicting human resting-state functional connectivity from structural connectivity. *Proceedings of the National Academy of Sciences*, 106(6):2035–2040, February 2009.
- [29] G. Deco and V. K. Jirsa. Ongoing cortical activity at rest: Criticality, multistability, and ghost attractors. *Journal of Neuroscience*, 32(10):3366–3375, March 2012.
- [30] Ed Bullmore and Olaf Sporns. Complex brain networks: graph theoretical analysis of structural and functional systems. *Nature Reviews Neuroscience*, 10(3):186–198, February 2009.
- [31] Gustavo Deco, Adrián Ponce-Alvarez, Patric Hagmann, Gian Luca Romani, Dante Mantini, and Maurizio Corbetta. How local excitation–inhibition ratio impacts the whole brain dynamics. *Journal of Neuroscience*, 34(23):7886–7898, 2014.
- [32] Gustavo Deco, Morten L. Kringelbach, Aurina Arnatkeviciute, Stuart Oldham, Kristina Sabarodin, Nigel C. Rogasch, Kevin M. Aquino, and Alex Fornito. Dynamical consequences of regional heterogeneity in the brain's transcriptional landscape. *Science Advances*, 7(29):eabf4752, July 2021.
- [33] Paula Sanz Leon, Stuart Knock, M. Woodman, Lia Domide, Jochen Mersmann, Anthony McIntosh, and Viktor Jirsa. The virtual brain: a simulator of primate brain network dynamics. *Frontiers in Neuroinformatics*, 7:10, 2013.
- [34] Ben H. Jansen and Vincent G. Rit. Electroencephalogram and visual evoked potential generation in a mathematical model of coupled cortical columns. *Biological Cybernetics*, 73(4):357–366, September 1995.
- [35] Joana Cabral, Morten L. Kringelbach, and Gustavo Deco. Functional connectivity dynamically evolves on multiple time-scales over a static structural connectome: Models and mechanisms. *NeuroImage*, 160:84–96, October 2017.

- [36] G. Deco, A. Ponce-Alvarez, D. Mantini, G. L. Romani, P. Hagmann, and M. Corbetta. Resting-state functional connectivity emerges from structurally and dynamically shaped slow linear fluctuations. *Journal of Neuroscience*, 33(27):11239–11252, July 2013.
- [37] Andrew Zalesky, Alex Fornito, Ian H. Harding, Luca Cocchi, Murat Yücel, Christos Pantelis, and Edward T. Bullmore. Whole-brain anatomical networks: Does the choice of nodes matter? *NeuroImage*, 50(3):970–983, April 2010.
- [38] Jesper L. R. Andersson, Mark S. Graham, Enikő Zsoldos, and Stamatis N. Sotiropoulos. Incorporating outlier detection and replacement into a non-parametric framework for movement and distortion correction of diffusion MR images. *NeuroImage*, 141:556–572, November 2016.
- [39] Kathryn P. Riley, David A. Snowden, and William R. Markesbery. Alzheimer's neurofibrillary pathology and the spectrum of cognitive function: Findings from the nun study. *Annals of Neurology*, 51(5):567–577, apr 2002.
- [40] Peng Wang, Ru Kong, Xiaolu Kong, Raphaël Liégeois, Csaba Orban, Gustavo Deco, Martijn P. van den Heuvel, and B.T. Thomas Yeo. Inversion of a large-scale circuit model reveals a cortical hierarchy in the dynamic resting human brain. *Science Advances*, 5(1):eaat7854, January 2019.
- [41] Rishidev Chaudhuri, Kenneth Knoblauch, Marie-Alice Gariel, Henry Kennedy, and Xiao-Jing Wang. A large-scale circuit mechanism for hierarchical dynamical processing in the primate cortex. *Neuron*, 88(2):419–431, October 2015.
- [42] Pablo Núñez, Jesús Poza, Carlos Gómez, Víctor Rodríguez-González, Arjan Hillebrand, Miguel A Tola-Arribas, Mónica Cano, and Roberto Hornero. Characterizing the fluctuations of dynamic resting-state electrophysiological functional connectivity: reduced neuronal coupling variability in mild cognitive impairment and dementia due to alzheimer's disease. *Journal of Neural Engineering*, 16(5):056030, September 2019.
- [43] Gustavo Deco, Morten L. Kringelbach, Viktor K. Jirsa, and Petra Ritter. The dynamics of resting fluctuations in the brain: metastability and its dynamical cortical core. *Scientific Reports*, 7(1), June 2017.
- [44] Matthew F. Glasser, Stamatis N. Sotiropoulos, J. Anthony Wilson, Timothy S. Coalson, Bruce Fischl, Jesper L. Andersson, Junqian Xu, Saad Jbabdi, Matthew Webster, Jonathan R. Polimeni, David C. Van Essen, and Mark Jenkinson. The minimal preprocessing pipelines for the human connectome project. *NeuroImage*, 80:105–124, October 2013.
- [45] Martin Reuter, Nicholas J. Schmansky, H. Diana Rosas, and Bruce Fischl. Within-subject template estimation for unbiased longitudinal image analysis. *NeuroImage*, 61(4):1402–1418, July 2012.
- [46] Stephen M. Smith, Mark Jenkinson, Mark W. Woolrich, Christian F. Beckmann, Timothy E.J. Behrens, Heidi Johansen-Berg, Peter R. Bannister, Marilena De Luca, Ivana Drobnyak, David E. Flitney, Rami K. Niazy, James Saunders, John Vickers, Yongyue Zhang, Nicola De Stefano, J. Michael Brady, and Paul M. Matthews. Advances in functional and structural MR image analysis and implementation as FSL. *NeuroImage*, 23:S208–S219, January 2004.
- [47] Mark W. Woolrich, Saad Jbabdi, Brian Patenaude, Michael Chappell, Salima Makni, Timothy Behrens, Christian Beckmann, Mark Jenkinson, and Stephen M. Smith. Bayesian analysis of neuroimaging data in FSL. *NeuroImage*, 45(1):S173–S186, March 2009.
- [48] Mark Jenkinson, Christian F. Beckmann, Timothy E.J. Behrens, Mark W. Woolrich, and Stephen M. Smith. FSL. *NeuroImage*, 62(2):782–790, August 2012.
- [49] Matthew F. Glasser, Timothy S. Coalson, Emma C. Robinson, Carl D. Hacker, John Harwell, Essa Yacoub, Kamil Ugurbil, Jesper Andersson, Christian F. Beckmann, Mark Jenkinson, Stephen M. Smith, and David C. Van Essen. A multi-modal parcellation of human cerebral cortex. *Nature*, 536(7615):171–178, July 2016.
- [50] Emma C. Robinson, Saad Jbabdi, Matthew F. Glasser, Jesper Andersson, Gregory C. Burgess, Michael P. Harms, Stephen M. Smith, David C. Van Essen, and Mark Jenkinson. MSM: A new flexible framework for multimodal surface matching. *NeuroImage*, 100:414–426, October 2014.
- [51] Jelle Veraart, Dmitry S. Novikov, Daan Christiaens, Benjamin Ades-aron, Jan Sijbers, and Els Fieremans. Denoising of diffusion MRI using random matrix theory. *NeuroImage*, 142:394–406, November 2016.
- [52] J.-Donald Tournier, Fernando Calamante, and Alan Connelly. Determination of the appropriate value and number of gradient directions for high-angular-resolution diffusion-weighted imaging. *NMR in Biomedicine*, 26(12):1775–1786, August 2013.
- [53] J.-Donald Tournier, Fernando Calamante, and Alan Connelly. Robust determination of the fibre orientation distribution in diffusion MRI: Non-negativity constrained super-resolved spherical deconvolution. *NeuroImage*, 35(4):1459–1472, May 2007.

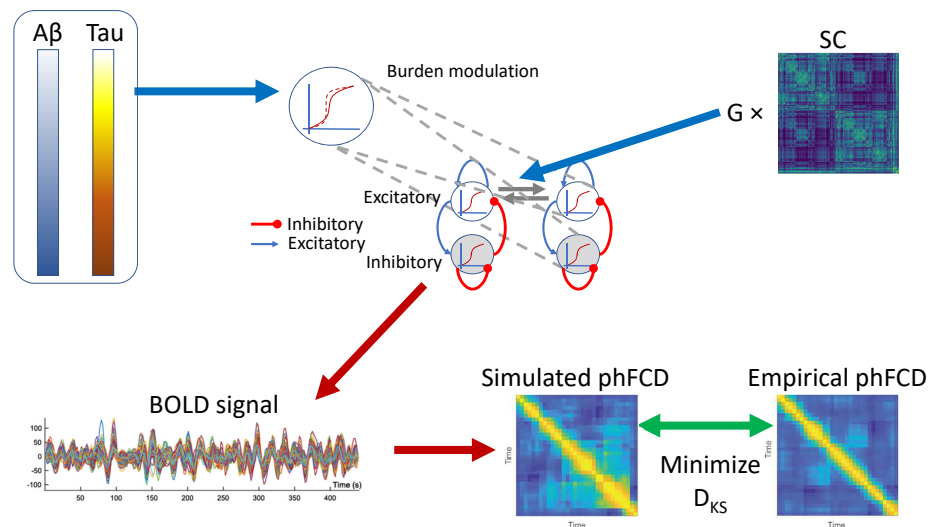
- [54] J Donald Tournier, Fernando Calamante, and Alan Connelly. Improved probabilistic streamlines tractography by 2nd order integration over fibre orientation distributions. In *Proceedings of the international society for magnetic resonance in medicine*, volume 18, page 1670, 2010.
- [55] Robert E. Smith, Jacques-Donald Tournier, Fernando Calamante, and Alan Connelly. SIFT2: Enabling dense quantitative assessment of brain white matter connectivity using streamlines tractography. *NeuroImage*, 119:338–351, October 2015.
- [56] Robert E. Smith, Jacques-Donald Tournier, Fernando Calamante, and Alan Connelly. Anatomically-constrained tractography: Improved diffusion MRI streamlines tractography through effective use of anatomical information. *NeuroImage*, 62(3):1924–1938, September 2012.
- [57] Thomas M. J. Fruchterman and Edward M. Reingold. Graph drawing by force-directed placement. *Software: Practice and Experience*, 21(11):1129–1164, November 1991.
- [58] K.-F. Wong and X.-J. Wang. A recurrent network mechanism of time integration in perceptual decisions. *Journal of Neuroscience*, 26(4):1314–1328, January 2006.
- [59] Klaas Enno Stephan, Lars Kasper, Lee M. Harrison, Jean Daunizeau, Hanneke E.M. den Ouden, Michael Breakspear, and Karl J. Friston. Nonlinear dynamic causal models for fMRI. *NeuroImage*, 42(2):649–662, August 2008.
- [60] Hongjun Fu, Andrea Possenti, Rosie Freer, Yoshikazu Nakano, Nancy C. Hernandez Villegas, Maoping Tang, Paula V. M. Cauhy, Benjamin A. Lassus, Shuo Chen, Stephanie L. Fowler, Helen Y. Figueroa, Edward D. Huey, Gail V. W. Johnson, Michele Vendruscolo, and Karen E. Duff. A tau homeostasis signature is linked with the cellular and regional vulnerability of excitatory neurons to tau pathology. *Nature Neuroscience*, 22(1):47–56, December 2018.
- [61] Jorge J. Palop and Lennart Mucke. Network abnormalities and interneuron dysfunction in alzheimer disease. *Nature Reviews Neuroscience*, 17(12):777–792, November 2016.
- [62] Benedikt Zott, Manuel M. Simon, Wei Hong, Felix Unger, Hsing-Jung Chen-Engerer, Matthew P. Frosch, Bert Sakmann, Dominic M. Walsh, and Arthur Konnerth. A vicious cycle of β amyloid-dependent neuronal hyperactivation. *Science*, 365(6453):559–565, August 2019.
- [63] Joseph McInnes, Keimpe Wierda, An Snellinx, Laura Bounti, Yu-Chun Wang, Ilie-Cosmin Stancu, Nuno Apóstolo, Kris Gevaert, Ilse Dewachter, Tara L. Spires-Jones, Bart De Strooper, Joris De Wit, Lujia Zhou, and Patrik Verstreken. Synaptogyrin-3 mediates presynaptic dysfunction induced by tau. *Neuron*, 97(4):823–835.e8, February 2018.
- [64] Bruno Vasconcelos, Ilie-Cosmin Stancu, Arjan Buist, Matthew Bird, Peng Wang, Alexandre Vanoosthuyse, Kristof Van Kolen, An Verheyen, Pascal Kienlen-Campard, Jean-Noël Octave, Peter Baatsen, Diederik Moechars, and Ilse Dewachter. Heterotypic seeding of tau fibrillization by pre-aggregated abeta provides potent seeds for prion-like seeding and propagation of tau-pathology in vivo. *Acta Neuropathologica*, 131(4):549–569, January 2016.
- [65] Sarah L Griner, Paul Seidler, Jeannette Bowler, Kevin A Murray, Tianxiao Peter Yang, Shruti Sahay, Michael R Sawaya, Duilio Cascio, Jose A Rodriguez, Stephan Philipp, Justyna Sosna, Charles G Glabe, Tamir Gonen, and David S Eisenberg. Structure-based inhibitors of amyloid beta core suggest a common interface with tau. *eLife*, 8:e46924, oct 2019.
- [66] Ünal Sakoğlu, Godfrey D. Pearlson, Kent A. Kiehl, Y. Michelle Wang, Andrew M. Michael, and Vince D. Calhoun. A method for evaluating dynamic functional network connectivity and task-modulation: application to schizophrenia. *Magnetic Resonance Materials in Physics, Biology and Medicine*, 23(5-6):351–366, February 2010.
- [67] Daniel A. Handwerker, Vinai Roopchansingh, Javier Gonzalez-Castillo, and Peter A. Bandettini. Periodic changes in fMRI connectivity. *NeuroImage*, 63(3):1712–1719, November 2012.
- [68] David T. Jones, Prashanthi Vemuri, Matthew C. Murphy, Jeffrey L. Gunter, Matthew L. Senjem, Mary M. Machulda, Scott A. Przybelski, Brian E. Gregg, Kejal Kantarci, David S. Knopman, Bradley F. Boeve, Ronald C. Petersen, and Clifford R. Jack. Non-stationarity in the “resting brain’s” modular architecture. *PLoS ONE*, 7(6):e39731, June 2012.
- [69] R. Matthew Hutchison, Thilo Womelsdorf, Joseph S. Gati, Stefan Everling, and Ravi S. Menon. Resting-state networks show dynamic functional connectivity in awake humans and anesthetized macaques. *Human Brain Mapping*, 34(9):2154–2177, March 2012.
- [70] Enrique C.A. Hansen, Demian Battaglia, Andreas Spiegler, Gustavo Deco, and Viktor K. Jirsa. Functional connectivity dynamics: Modeling the switching behavior of the resting state. *NeuroImage*, 105:525–535, January 2015.
- [71] R. Matthew Hutchison, Thilo Womelsdorf, Elena A. Allen, Peter A. Bandettini, Vince D. Calhoun, Maurizio Corbetta, Stefania Della Penna, Jeff H. Duyn, Gary H. Glover, Javier Gonzalez-Castillo, Daniel A. Handwerker, Shella Keilholz, Vesa Kiviniemi, David A. Leopold, Francesco de Pasquale, Olaf Sporns, Martin Walter, and Catie Chang. Dynamic functional connectivity: Promise, issues, and interpretations. *NeuroImage*, 80:360–378, October 2013.

- [72] Nora Leonardi and Dimitri Van De Ville. On spurious and real fluctuations of dynamic functional connectivity during rest. *NeuroImage*, 104:430–436, January 2015.
- [73] Andrew Zalesky and Michael Breakspear. Towards a statistical test for functional connectivity dynamics. *NeuroImage*, 114:466–470, July 2015.
- [74] Timothy O. Laumann, Abraham Z. Snyder, Anish Mitra, Evan M. Gordon, Caterina Gratton, Babatunde Adeyemo, Adrian W. Gilmore, Steven M. Nelson, Jeff J. Berg, Deanna J. Greene, John E. McCarthy, Enzo Tagliazucchi, Helmut Laufs, Bradley L. Schlaggar, Nico U. F. Dosenbach, and Steven E. Petersen. On the stability of BOLD fMRI correlations. *Cerebral Cortex*, 27(10):4719–4732, 09 2016.
- [75] Maria Giulia Preti, Thomas AW Bolton, and Dimitri Van De Ville. The dynamic functional connectome: State-of-the-art and perspectives. *NeuroImage*, 160:41–54, October 2017.
- [76] Enrico Glerean, Juha Salmi, Juha M. Lahnakoski, Iiro P. Jääskeläinen, and Mikko Sams. Functional magnetic resonance imaging phase synchronization as a measure of dynamic functional connectivity. *Brain Connectivity*, 2(2):91–101, April 2012.
- [77] Adrián Ponce-Alvarez, Gustavo Deco, Patric Hagmann, Gian Luca Romani, Dante Mantini, and Maurizio Corbetta. Resting-state temporal synchronization networks emerge from connectivity topology and heterogeneity. *PLOS Computational Biology*, 11(2):e1004100, February 2015.
- [78] Gustavo Deco and Morten Kringelbach. Metastability and coherence: Extending the communication through coherence hypothesis using a whole-brain computational perspective. *Trends in Neurosciences*, 39(6):432, June 2016.

*Data used in preparation of this article were obtained from the Alzheimer's Disease Neuroimaging Initiative (ADNI) database (adni.loni.usc.edu). As such, the investigators within the ADNI contributed to the design and implementation of ADNI and/or provided data but did not participate in analysis or writing of this report. A complete listing of ADNI investigators can be found at: https://adni.loni.usc.edu/wp-content/uploads/how_to_apply/ADNI_Acknowledgement_List.pdf



(a) Integrating protein burden data



(b) Fitting the phFCD in the whole-brain model

Figure 1. Illustrative overview of our processing pipeline. (a) Basic ingredients for the integration of protein burden data from structural (dMRI, top left), functional (fMRI, top right), and burden (PET, right) using the same parcellation for each neuroimaging modality (top, middle) for generating a whole-brain computational model (bottom left). Each node of the model is using a realistic underlying biophysical neuronal model including AMPA, GABA, and NMDA synapses as well as neurotransmitter gain modulation of these. (b) Fitting the measures in the whole-brain model: First, we simulate the BOLD timeseries for each brain region in the parcellation, for each subject. These timeseries are defined by its inputs, namely a previously found global coupling constant G , an individual Structural Connectivity (SC) matrix, and the corresponding individual $A\beta$ and tau burdens. Subsequently, we compute a time-versus-time matrix of phFCD. This is compared to a reference empirical phFCD for that same subject using the Kolmogorov-Smirnov distance (KS), D_{KS} , which is minimized to find the generative parameters of the model. This process is repeated for the other two measures already mentioned, FC and swFCD.

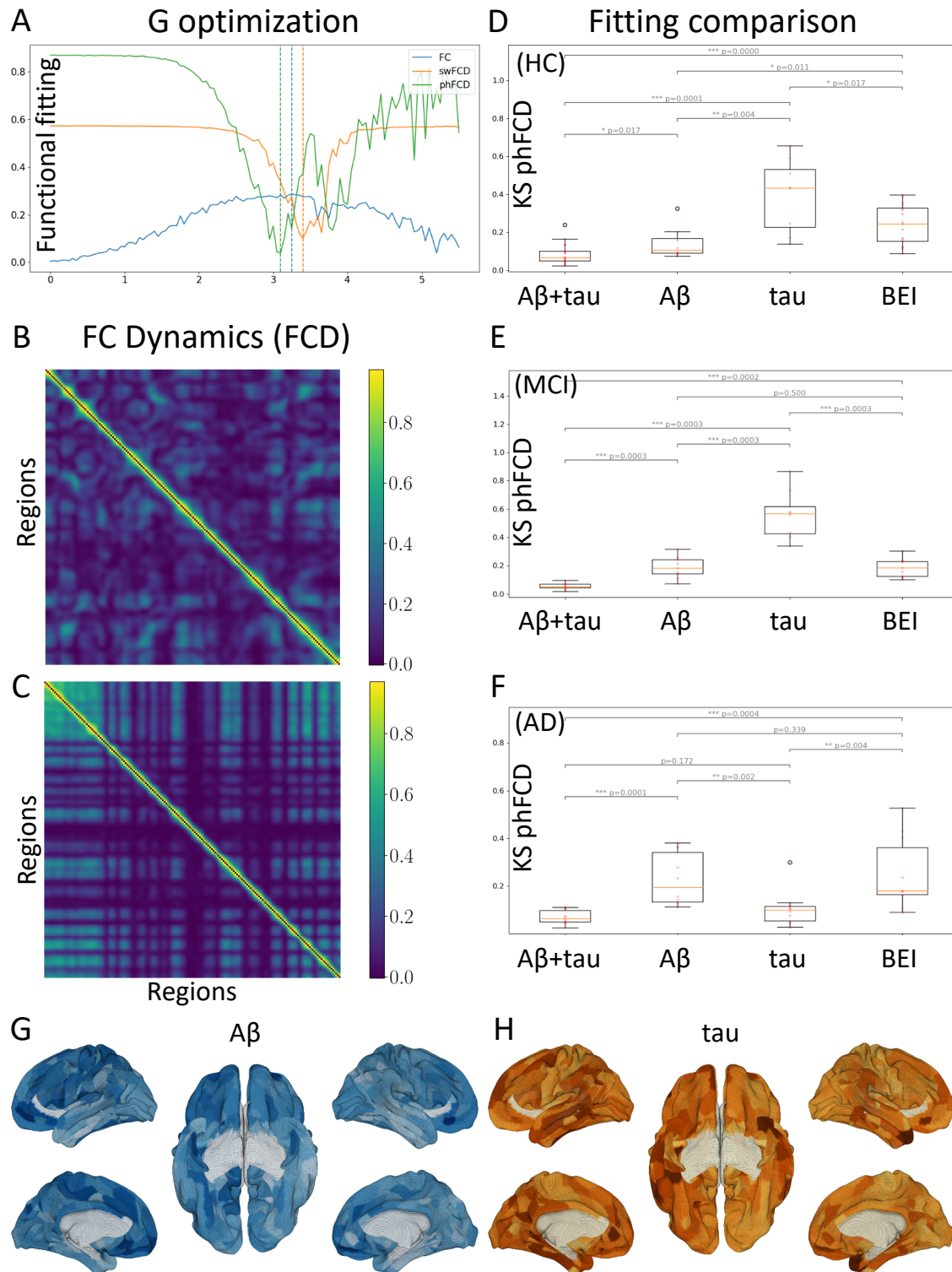


Figure 2. Optimization and evaluation of the model: First, using only HC subjects, the global coupling parameter is found, and then the model free parameters are adjusted to minimize the distance between the empirical and simulated fMRI data, taking into account the regional burden distributions. (A) Minimization of the global coupling parameter G between 0 and 5.5, for Functional connectivity (FC), sliding-window Functional connectivity Dynamics (swFCD) and phase FCD (phFCD). Given their strong similarity in the results, phFCD was used for all subsequent computations. (B, C) Shows the normalized (in $[0, 1]$) FCD distributions for the empirical data (top) and the simulated model (bottom). For an exemplary resulting timeseries, please refer to the bottom-left part of Figure 1b. (D, E, F): Analysis of the impact (smaller values are better) of the different burdens when optimized in isolation with respect to their impact in the phFCD (KS distance), and with respect to the homogeneous state as a reference. As can be seen, the results for AD clearly show that tau alone accounts for the vast majority of the weight of the impact on brain activity, while for MCI patients it is $A\beta$ who dominates. The case for HC patients is not so clear, but we also see a predominance of $A\beta$, although in a less conclusive manner. (G) $A\beta$ and (H) Tau burdens of one subject (036_S_4430 in ADNI's database). Colors correspond to the normalized burden of each protein.

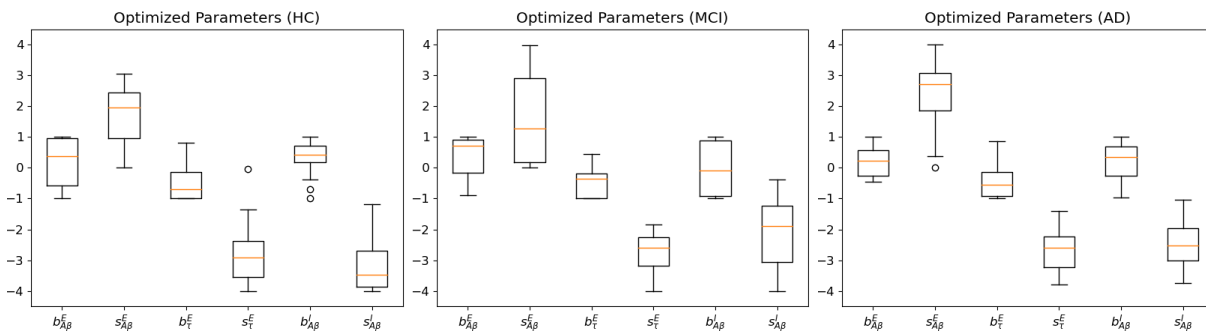


Figure 3. Parameter values found after the optimization stage for HC, MCI and AD subjects. Observe that all $b_{(A\beta, \tau)}^{(E,I)}$, the excitatory/inhibitory A β and tau bias parameters, have negligible values, while the scaling parameters $s_{(A\beta, \tau)}^{(E,I)}$ present non-null values. Of note, the p-values between the different scaling parameters across the cohorts are different in a moderately significant way ($p < 0.03$), remarkably between HC and AD, but usually not between MCI and AD. In these plots, boxes extend from the lower to upper quartile values of the data, adding an orange line at the median. Also, whiskers are used to show the range of the data, extending from the box.

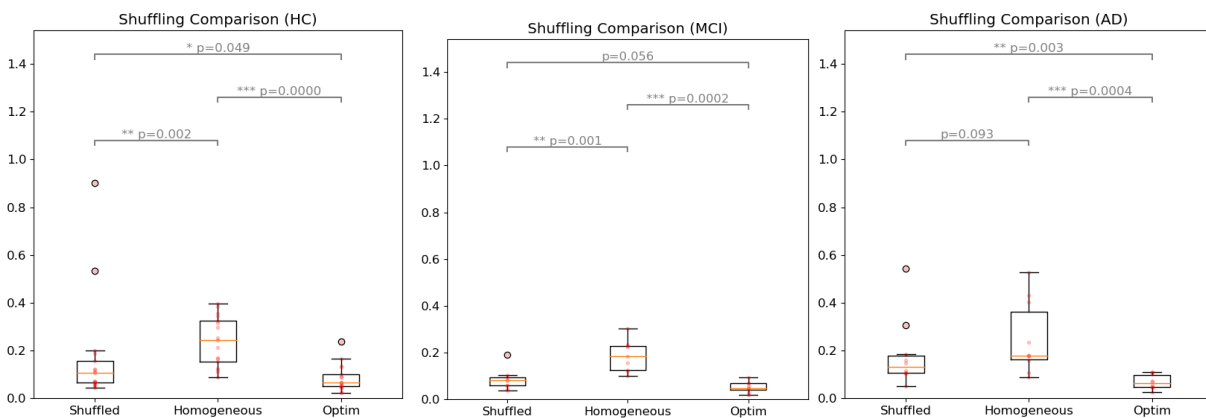


Figure 4. Comparison between the homogeneous model, the result obtained and the same parameter values but with shuffled burdens. As can be seen, the differences in fit statistics between models are significant. In particular, for the AD cohort, the median phFCD correlation between model and data showed $r < 0.1$ for the heterogeneous model, and $r \approx 0.2$ for the BEI model. In all subject groups, the difference between these two models is clear, with $p < 0.0005$.

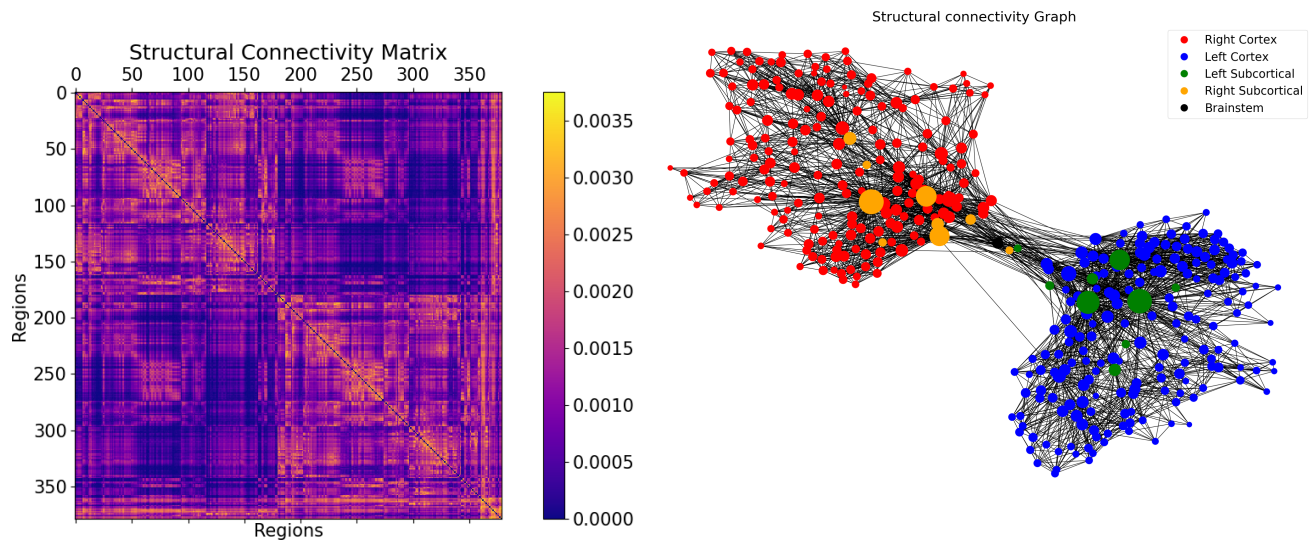


Figure 5. Visualization of the SC graph, in matrix form (left) and as a graph showing the strongest 5% of connections. Node positions are computed with Fruchterman and Reingold's [57] algorithm, which assumes stronger forces between tightly connected nodes. Besides the high degree of symmetry, we can observe the laterality is kept in the graph structure (also for subcortical regions). Node size linearly represents the graph theoretical measure of structural degree for each node. As we can see, the most important hubs are in the subcortical regions.

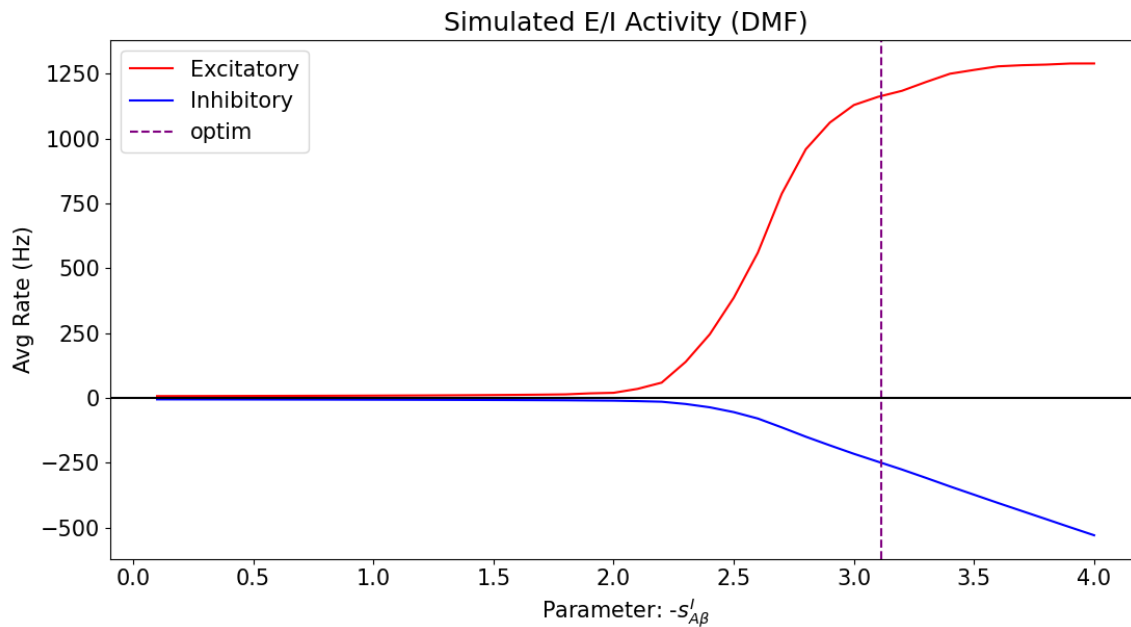


Figure 6. Excitatory and inhibitory mean firing rates as a function of the $A\beta$ inhibitory scaling s_{AB}^I , with all the other parameters of the model at the (averaged) fitted optimum values. For the purpose of clarity, the horizontal axis for the scaling has been taken as absolute values, to illustrate the behavior with increasing $A\beta$ loads. The vertical axis shows the firing rates of both excitatory and inhibitory populations. It can be clearly seen that the net effect of the burden is to increase the overall region firing rate, measured at the excitatory population. For the sake of clarity, the inhibitory firing rate has been vertically inverted (negated) to show their decreased effect on the excitatory population, thus confirming previous findings [21]. The vertical discontinuous line shows the optimum found for s_{AB}^I .